Thin Solid Films 517 (2009) 6635–6641

Contents lists available at ScienceDirect

Thin Solid Films

journal homepage: www.elsevier.com/locate/tsf

# Compositional and structural evolution of sputtered Ti-Al-N

Li Chen [a,b,*], Martin Moser [a], Yong Du [b], Paul H. Mayrhofer [a]

[a] Department of Physical Metallurgy and Materials Testing, Montanuniversität Leoben, Leoben, 8700, Austria
[b] State Key Laboratory of Powder Metallurgy, Central South University, Changsha Hunan, 410083, China

ARTICLE INFO

*Article history:*
Received 13 March 2009
Received in revised form 21 April 2009
Accepted 22 April 2009
Available online 3 May 2009

*Keywords:*
Physical vapour deposition (PVD)
Ti-Al-N
Reactive sputtering
Composition

ABSTRACT

The compositional and structural evolution of Ti-Al-N thin films as a function of the total working gas pressure ($p_T$), the $N_2$-to-total pressure ratio ($p_{N2}/p_T$), the substrate-to-target distance (ST), the substrate position, the magnetron power current ($I_m$), the externally applied magnetic field, and the energy and the ion-to-metal flux ratio of the ion bombardment during reactive sputtering of a $Ti_{0.5}Al_{0.5}$ target is investigated in detail. Based on this variation we propose that the different poisoning states of the Ti and Al particles of the powder-metallurgically prepared $Ti_{0.5}Al_{0.5}$ target in addition to scattering and angular losses of the sputter flux cause a significant modification in the Al/Ti ratio of the deposited thin films ranging from ~1.05 to 2.15.

The compositional variation induces a corresponding structural modification between single-phase cubic, mixed cubic-hexagonal and single-phase hexagonal. However, the maximum Al content for single-phase cubic $Ti_{1-x}Al_xN$ strongly depends on the deposition conditions and was obtained with $x = 0.66$, for the coating deposited at 500 °C, $p_T = 0.4$ Pa, ST = 85 mm, and $p_{N2}/p_T = 17\%$. Our results show, that in particular, the $N_2$-to-total pressure ratio in combination with the sputtering power density of the $Ti_{0.5}Al_{0.5}$ compound target has a pronounced effect on the Al/Ti ratio and the structure development of the coatings prepared.



## 1. Introduction

Magnetron sputtering of thin films is a major field of physical vapor deposition (PVD) technologies [1–5], where various material combinations and compounds are accessible. In general, compound films can be prepared by reactive sputtering, where in addition to the sputtered target material a reactive gas like $N_2$ is introduced to the PVD chamber, or by sputtering of a compound target itself [6–9]. Due to the massive move in industry and research from binary to ternary and further towards multinary systems, compound target development became a major field for PVD [10–17]. While it is noticed that the composition of the coating can vary from that of the corresponding target [18–22] depending on the deposition conditions used, such as gas flow, sputtering power, substrate bias, etc., little is understood on the origin of these influences. In order to benefit from these effects of deposition-parameters-induced variations in coating composition, with respect to the corresponding compound target, we use a model-system, Ti-Al-N, for detailed studies of their compositional and structural evolution as a function of specific parameters during unbalanced magnetron sputtering.

Ti-Al-N hard coatings with cubic NaCl (c) structure, where Al substitutes for Ti in the TiN based structure (i.e., $Ti_{1-x}Al_xN$), are widely used for wear resistant applications like cutting tools, due to their unique properties, such as high temperature oxidation resistance and age-hardening abilities [23–29]. The chemical composition of Ti-Al-N thin films depends to a great extent on the deposition parameters, which basically determine their structure and properties [30–33]. Single phase cubic Ti-Al-N films with high Al contents exhibit excellent mechanical properties and oxidation resistance. For Al contents exceeding the cubic solid solubility, which is reported with $x$ being in the range of 0.65-0.75, a mixed cubic-NaCl and hexagonal-ZnS (h-AlN) structure is formed, which results in reduced film properties, e.g., decreasing hardness, bulk-, elastic-, and shear-moduli, as well as wear resistance [11,26–33]. Therefore, the compositional variation of Ti-Al-N films, arising from the deposition parameters, influence their structure evolution and mechanical properties. Extensive studies of the correlation between film composition, structure and performance of Ti-Al-N films deposited by magnetron sputtering have already been reported [10–17]. However, only little is known and understood on the correlation between deposition parameters during reactive sputtering of a compound target and the resulting film composition and structure.

To study the effect of various deposition parameters on the composition and structure of Ti-Al-N thin films we varied the total working gas pressure ($p_T$), the ratio of the $N_2$-partial pressure ($p_{N2}$) to total pressure ($p_{N2}/p_T$), the substrate-to-target distance (ST), the substrate position with respect to the center of substrate holder (SP), which is above the center of the parallel aligned target, the magnetron power current ($I_m$), the externally applied magnetic field ($B_{ext}$), the ion energy ($E_i$), and the ion-to-metal flux ratio ($J_{ion}/J_{me}$).

## 2. Experimental details

Ti-Al-N films were deposited onto Si substrates ($20 \times 7 \times 0.3$ mm$^3$) by unbalanced magnetron sputtering from a powder-metallurgically

* Corresponding author. Tel.: +43 3842 402 4236; fax: +43 3842 402 737.
*E-mail address:* li.chen@unileoben.ac.at (L. Chen).

0040-6090/$ – see front matter. 
doi:10.1016/j.tsf.2009.04.056

**Table 1**
Total working gas pressure ($p_T$), $N_2$-to-total pressure ratio ($p_{N2}/p_T$), substrate-to-target distance (ST), distance of the substrate to the center of the substrate holder (SP), magnetron power current ($I_m$), externally applied magnetic field ($B_{ext}$), applied substrate bias potential ($V_b$), and ion energy ($E_i$) used during deposition.

| $p_{N2}/p_T$ (%) | $p_T$ (Pa) | ST (mm) | SP (mm) | $I_m$ (A) | $\pm B_{ext}$ (G) | $-V_b$ (V) | $E_i$ (eV) |
|---|---|---|---|---|---|---|---|
| 0–100 | 0.4 | 85 | 32 | 1.5 | −40 | 60 | 43 |
| 17 | 0.4–2.24 | 85 | 32 | 1.5 | −40 | 60 | 43 |
| 17, 23 | 0.4 | 57–85 | 32 | 1.5 | −40 | 60 | 43 |
| 0, 17, 100 | 0.4 | 85 | 0–80 | 1.5 | −40 | 60 | 43 |
| 27 | 0.4 | 85 | 32 | 1.5–4.0 | −40 | 60 | 43 |
| 17 | 0.4 | 85 | 0 | 1.5 | −120–+120 | 30–86 | 30 |
| 17 | 0.4 | 85 | 0 | 1.5 | −40 | 37–112 | 20–95 |
| 0, 100 | 4 | 85 | 32 | 1.5 | −40 | 60 | 43 |

Chen et al.

prepared $Ti_{0.5}Al_{0.5}$ compound target (diameter of 152 mm and purity of 99.9%, PLANSEE) in a mixed Ar + $N_2$ (both of 99.999% purity) glow discharge. More details on the magnetron sputtering system used are described in Ref. [34]. Prior to the deposition with a constant substrate temperature ($T_s$) of 500 °C and a base pressure ≤0.8 mPa, the substrates were etched for 20 min using an $Ar^+$ glow discharge with ~1250 V and 25 mA, at a pressure of 3.0 Pa. Before loading the chamber, the polished Si substrates were ultra-sonically cleaned in acetone and ethylene. The total working gas pressure $p_T$ was varied between 0.4 and 4 Pa, the $N_2$-to-total pressure ratio $p_{N2}/p_T$ was varied between 0 and 100%, the substrate-to-target distance ST was varied between 57 and 85 mm, the substrate distance to the center of the substrate holder SP was varied between 0 and 80 mm, the magnetron power current $I_m$ was varied between 1.5 and 4.0 A, and the ion energy $E_i$ was varied between 20 and 95 eV.

The externally applied magnetic field ($B_{ext}$) using a pair of Helmholtz coils was varied between − 120 and + 120 G. This notification refers to a broadening (−) or concentration (+) of the sputtering zone at the target surface and the plasma zone at the substrate holder by influencing the permanent magnetic field of the planar magnetron.

The plasma characteristics like ion flux $J_{ion}$ and plasma potential $V_p$, were determined by Hiden ESP Langmuir wire probe measurements following the procedures described in Refs. [35,36]. The metal flux $J_{me}$ was estimated from the deposition rate ($R$), which itself was calculated from the film thickness, measured by the ball crater method, deposition time, and assuming a theoretical density for cubic $Ti_{1-x}Al_xN$ [37–39]. The ion energy can be estimated from the difference between the plasma potential ($V_p$) and the substrate bias potential ($V_b$) with $E_i = e(V_p - V_b)$ [40]. Details on the deposition parameters are presented in Table 1, and the schematic of the substrate holder and target arrangement is given in Fig. 1.

The chemical composition of the films was determined using energy dispersive X-ray analysis (EDX) with an Oxford Instruments INCA EDX unit attached to a scanning electron microscopy (SEM) operated with 25 kV. Structural investigations were conducted by X-ray diffraction (XRD) with $CuK_\alpha$ radiation using a Bruker D8 in Bragg/Brentano mode.

## 3. Results and discussion

### 3.1. Plasma characteristics and deposition rate

Increasing the $N_2$-to-total pressure ratio $p_{N2}/p_T$ from 0 to 100% at a constant total pressure of 0.4 Pa induces a reduction in deposition rate from 59 to 9 nm/min. The strong change in the dependence of the deposition rate on the $N_2$-to-total pressure ratio suggests a change in sputtering mode from metallic towards poisoned in the $p_{N2}/p_T$ range 17–23%, see Fig. 2a. However, $J_{ion}/J_{me}$ almost continuously increases from 0.5 to 5.0 and $V_p$ increases from −15.8 to −20.2 V when increasing $p_{N2}/p_T$ from 0 to 100%, respectively. The sputtering yields for Ti, Al, TiN, and AlN are ~0.5, 0.9, 0.1, and 0.2 using argon ions with an energy of 500 eV [21]. Consequently, nitridation of the target is responsible for a decrease in deposition rate. The degree of the target nitridation determined by the partial pressure of reactive gas $N_2$ plays a significant role in deposition rate. As shown in Fig. 2a, initially the deposition rate strongly decreases to 20 nm/min with increasing $p_{N2}/p_T$ to 15%, which indicates a transition of the target surface from metallic to nitridic. With increasing $p_{N2}/p_T$ to 23% the deposition rate only slightly decreases from 20 to 17 nm/min suggesting that the target is still in transition mode. For a further increase in $p_{N2}/p_T$ the deposition rate initially decreases more pronounced and then approaches to an almost constant value of ~10 for $p_{N2}/p_T \geq 60\%$, indicating a poisoned target surface, in agreement to Ref. [18,41]. Consequently, we have chosen a $p_{N2}/p_T$ ratio of 17% (within the transition mode) as the standard value for further investigations.

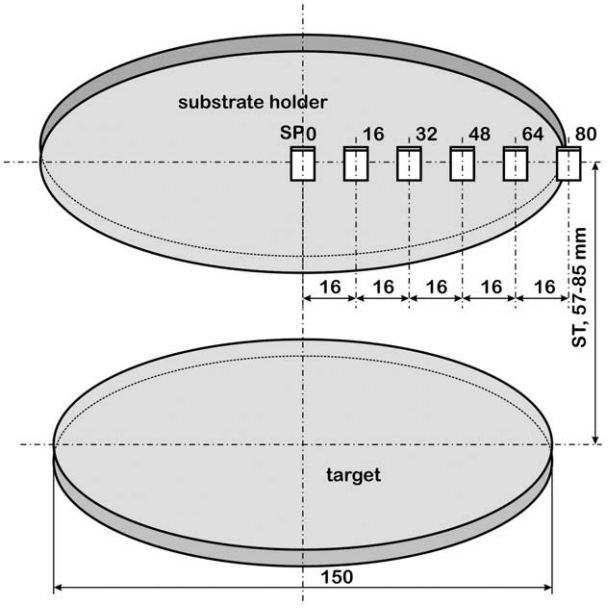


**Fig. 1.** Schematic of the substrate and target arrangement with indicated substrate-to-target distance ST and substrate position SP. Dimensions are given in mm.

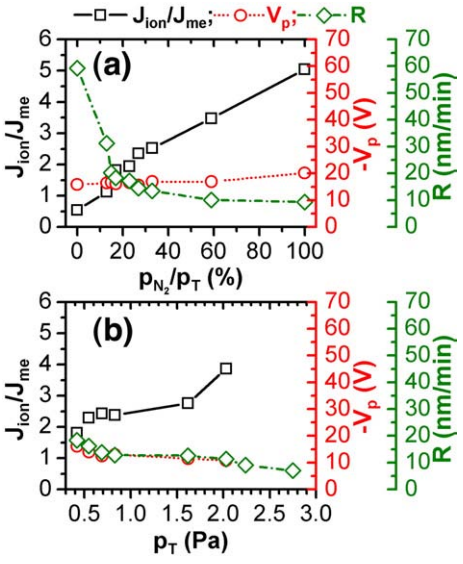


**Fig. 2.** Dependency of the incident ion-to-metal flux ratio ($J_{ion}/J_{me}$), plasma potential ($V_p$), and deposition rate ($R$) on the (a) $N_2$-to-total pressure ratio ($p_{N2}/p_T$) for $p_T = 0.4$ Pa, and the (b) total working gas pressure ($p_T$) for $p_{N2}/p_T = 17\%$. The additional deposition parameters used were kept constant: $T_s = 500$ °C, ST = 85 mm, SP = 32 mm, $I_m = 1.5$ A, $B_{ext} = -40$ G, and $E_i = 43$ eV.

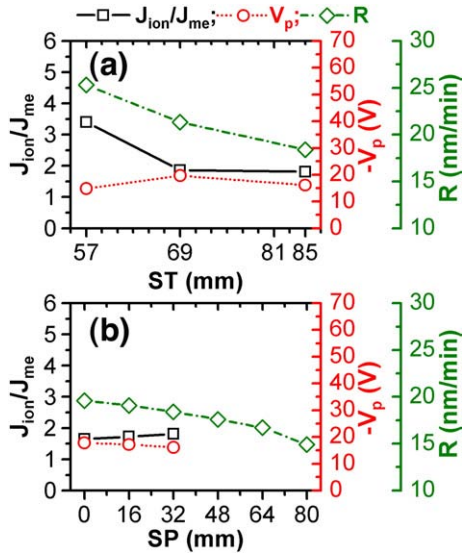


**Fig. 3.** Dependency of the incident ion-to-metal flux ratio ($J_{ion}/J_{me}$), plasma potential ($V_p$), and deposition rate ($R$) on the (a) substrate-to-target distance (ST) for SP = 32 mm, and the (b) substrate position (SP) for ST = 85 mm. The additional deposition parameters used were kept constant: $T_s$ = 500 °C, $p_{N2}/p_T$ = 17%, $p_T$ = 0.4 Pa, $I_m$ = 1.5 A, $B_{ext}$ = −40 G, and $E_i$ = 43 eV.

Increasing the total pressure from 0.4 to 2.8 Pa at constant $p_{N2}/p_T$ of 17% results in a decrease in deposition rate from 18 to 7 nm/min. This decreasing deposition rate with increasing total pressure $p_T$ can be attributed to increasing scattering losses as the mean free path MFP [22,42] ($MFP = \frac{1}{\sqrt{2}}\frac{k_B T}{p}\frac{1}{\pi(r_{Ar,N_2} + r_{Ti,Al})}$ with $k_B$ being Boltzmann's constant, $T$ the temperature, $p$ the pressure, and $r$ the covalent radius), decreases for Ti from ~95 to 14 mm and for Al from ~159 to 24 mm, when increasing $p_T$ from 0.4 to 2.8 Pa, respectively. The effect of target voltage variation in our experiments is minimal as it reduces only from 330 to 310 V when increasing $p_T$ from 0.4 to 2.8 Pa.

For the standard total pressure of 0.4 Pa, used for all other experiments, the MFP for Ti and Al is longer than the standard substrate-to-target distance ST of 85 mm. Consequently, scattering losses are minimal and further reduce when decreasing ST at constant $p_T$ and $p_{N2}/p_T$. As the substrates dive deeper into the denser plasma region when decreasing ST from 85 to 57 mm the ion-to-metal flux ratio increases from 1.8 to 3.4, see Fig. 3a, although the deposition rate increases from 18 to 25 nm/min. As the reduced scattering losses with decreasing ST can not account for the deposition rate increase, additional mechanisms are important such as the cosine emission distribution of the sputtered species [43–45]. The latter are responsible for an increased arrival rate of sputtered species at the substrate (which in our arrangement is small as compared to the target area) when decreasing ST. The angular distribution of the sputter flux is further investigated by varying the substrate position SP from 0 to 80 mm with respect to the center of the substrate holder (which is in line with the center of the parallel aligned target, see Fig. 1). Increasing SP from 0 to 80 mm causes a reduction of the deposition rate from 20 to 15 nm/min, see Fig. 3b, confirming a pronounced angular distribution of the sputter flux. With increasing SP, hence moving the substrate away from the target center, fewer target areas can provide particles that can reach the substrate.

Increasing the current supply for the target from 1.5 to 4.0 A increases the deposition rate from 15 to 53 nm/min, respectively, see Fig. 4a. To ensure, that also the coatings prepared with $I_m$ = 4 A are stoichiometric in nitrogen we used a $N_2$-to-total pressure ratio of 27% for this experiment. The pronounced increase in deposition rate from 23 to 38 nm/min when increasing $I_m$ from 2.5 to 3 A indicates a change in sputtering mode towards less poisoning, respectively. Nevertheless, $J_{ion}/J_{me}$ changes only between 2.2 and 1.6 and $V_p$ changes only between −15.5 and −16.7 V when increasing $I_m$ from 1.5 to 3 A, respectively.

When increasing the external magnetic field $B_{ext}$ from −120 to +120 G, which focuses the sputtering zone of the target towards the center, the ion-to-metal flux ratio $J_{ion}/J_{me}$ increases from 0.3 to 22.4 and the plasma potential $V_p$ increases from −0.6 to −63.6 V at the center of the substrate holder with ST = 85 mm, see Fig. 4b. This is in agreement to previous studies showing that the external magnetic field strongly influences $J_{ion}/J_{me}$ and $V_p$ [34,39]. The most pronounced increase in $J_{ion}/J_{me}$ from 1.7 to 18.8 and $V_p$ from −17.8 to −47.6 V is obtained with increasing $B_{ext}$ from −40 to +40 G. The deposition rate initially decreases from 31 nm/min with $B_{ext}$ = −120 G to the minimum value of 17 nm/min with $B_{ext}$ = 0 G, see Fig. 4b. The reduction in deposition rate, determined by the film thickness, can be attributed to changes in film-morphology from open columnar to fine columnar and dense. With increasing $J_{ion}/J_{me}$ the film becomes more dense and thereby suggests a lower deposition rate. Increasing $B_{ext}$ from 0 to +120 G causes a concentration of the glow discharge towards the center of the target, hence the average magnetron-power density increases, and thereby, also the deposition rate for the substrate above the target-center increases again from 17 to 32 nm/min.

### 3.2. Film composition and structure

The Ti-Al-N films investigated maintain always a higher Al/Ti ratio than the target for all deposition parameters used. Generally, sputter erosion from the compound target will produce an identical ratio of emitted Ti to Al atoms with that of the bulk target composition, considering no diffusion of the target elements [46]. The compositional deviation between our Ti-Al-N films and the $Ti_{0.5}Al_{0.5}$ target mainly derives from the different sputtering conditions for Al and Ti allowing angular and scattering losses. The decreased MFP value with increasing total pressure causes more collisions and in turn intensifies the scattering losses. To study the effect of scattering loss on the Al/Ti ratio of our films, we conducted sputtering experiments in Ar or $N_2$ atmosphere (i.e., $p_{N2}/p_T$ = 0 or 100%) with varying the total pressure. Increasing $p_T$ from 0.4 to 4 Pa results in a decrease of the Al/Ti ratio from 1.33 to 1.05 in Ar and from 1.57 to 1.22 in $N_2$. The reduction in Al/Ti with increasing $p_T$ in Ar or $N_2$ reveals that scattering losses are more

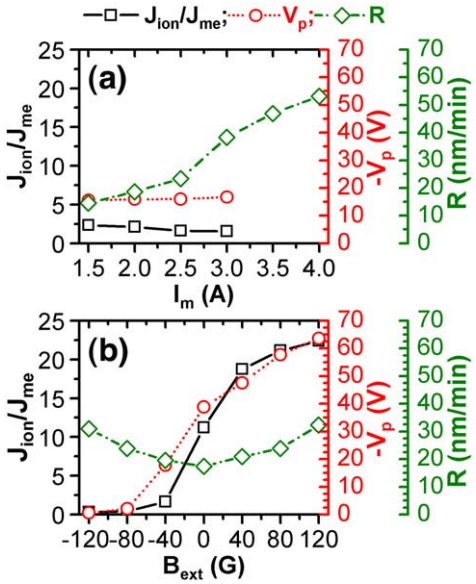


**Fig. 4.** Dependency of the incident ion-to-metal flux ratio ($J_{ion}/J_{me}$), plasma potential ($V_p$), and deposition rate ($R$) on the (a) magnetron power current ($I_m$) with $p_{N2}/p_T$ = 27%, SP = 32 mm, $B_{ext}$ = −40 G, and the (b) externally applied magnetic field ($B_{ext}$) with $p_{N2}/p_T$ = 17%, SP = 0 mm, $I_m$ = 1.5 A. The additional deposition parameters used were kept constant: $T_s$ = 500 °C, $p_T$ = 0.4 Pa, ST = 85 mm, and $E_i$ = 43 eV.

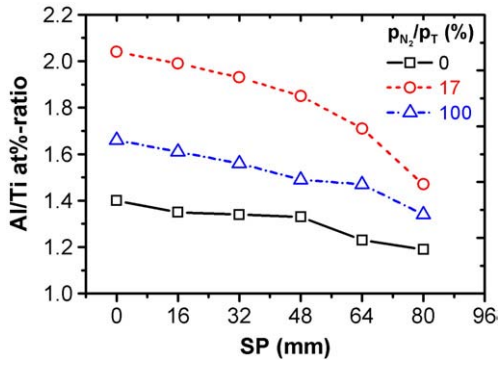


**Fig. 5.** Al/Ti ratio of the deposited films as a function of the substrate position SP for three different $N_2$-to-total pressure ratios of $p_{N2}/p_T = 0$, 17, and 100%, i.e., sputtering in Ar, Ar–$N_2$, and $N_2$ atmospheres, respectively. The additional deposition parameters used were kept constant: $T_s = 500$ °C, $p_T = 0.4$ Pa, ST = 85 mm, SP = 32 mm, $I_m = 1.5$ A, $B_{ext} = -40$ G, and $E_i = 43$ eV.

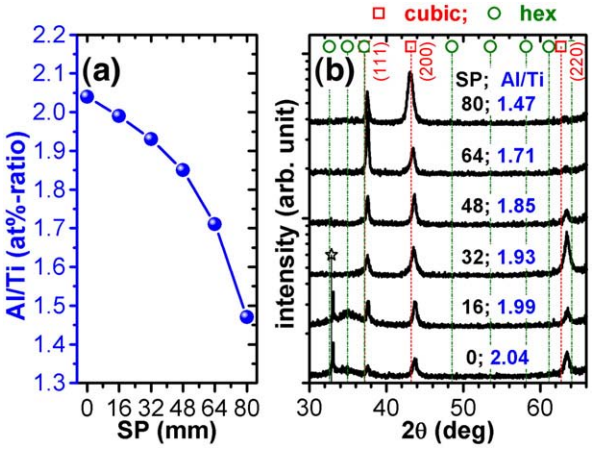


**Fig. 6.** (a) Al/Ti ratio and (b) XRD patterns of the $Ti_{1-x}Al_xN$ thin films as a function of the substrate position SP (mm) with $T_s = 500$ °C, $p_{N2}/p_T = 17\%$, $p_T = 0.4$ Pa, ST = 85 mm, $I_m = 1.5$ A, $B_{ext} = -40$ G, and $E_i = 43$ eV.

pronounced for the lighter Al atoms, although more scattering collisions occur for Ti due to its shorter MFP. The deviation in Ti/Al ratio between film and target at low total pressure can mainly be attributed to angular losses as scattering losses are minimal when the MFP is larger than the substrate-to-target distance ST.

As mentioned in the previous chapter the effect of angular losses is investigated by varying the substrate position SP from 0 to 80 mm from the substrate holder center (Fig. 1) using a total pressure $p_T$ of 0.4 Pa. As the Ti and Al particles from the $Ti_{0.5}Al_{0.5}$ target exhibit a different sputtering distribution, also the Al/Ti ratio of the films has a dependence on the substrate position SP, in addition to the deposition rate, compare Figs. 3b and 5. The decreasing Al/Ti ratios for $p_{N2}/p_T = 0$, 17 and 100% with increasing distance of the substrate position SP suggest a wider sputtering distribution for Al than for Ti in metallic or poisoned mode. In the center with SP = 0 the sputtering clouds around the radial race track exhibit the largest overlap and therefore the Al/Ti ratio is maximal. Also estimations by the SRIM code (sputtering ions: $Ar^+$ and $N_2^+$ with energy of 300, 350, 1000 eV) exhibit a larger angular sputtering distribution for Al as for Ti using $Ar^+$ and $N_2^+$ sputtering species with different energies.

Generally, the angular sputtering distribution depends on the target surface state as well as the energy and mass of the sputtering ions [47–49]. The films deposited within a mixed atmosphere with $p_{N2}/p_T = 17\%$ yield the highest value and the most pronounced decrease of Al/Ti ratio, which decreases from 2.04 to 1.47 with increasing the distance from the target center to 80 mm. Especially, when SP increases to values above 48 mm, the decrease is pronounced, see Fig. 5. This is attributed to different poisoning states of the Ti and Al target particles for $p_{N2}/p_T = 17\%$. As the Gibbs free energy for TiN with $\Delta G^0_{TiN} = -308.3$ kJ/mol is more negative than for AlN with $\Delta G^0_{AlN} = -287.0$ kJ/mol [50] the Ti particles of the powder-metallurgically prepared $Ti_{0.5}Al_{0.5}$ target are easier poisoned than the Al particles. Consequently, when the Ti particles are already poisoned, the Al particles can still be in metallic mode. This can explain the result of higher Al/Ti ratios when sputtering with $p_{N2}/p_T = 17\%$ as compared to sputtering in Ar or $N_2$ atmosphere, see Figs. 5 and 6a. The Ti-Al-N films deposited at the positions SP = 0 and 16 mm exhibit a hexagonal contribution to the cubic supersaturated $Ti_{1-x}Al_xN$ phase, due to the high Al/Ti ratio of 2.04 and 1.99, respectively, see Fig. 6b. By increasing SP to values above 32 mm the films exhibit a single-phase cubic structure, as thereby also the Al/Ti ratio decreases to values below 1.93.

This study already indicates that varying the $N_2$-to-total pressure ratio $p_{N2}/p_T$ at a constant total pressure $p_T$ of 0.4 Pa causes a pronounced change in Al/Ti ratio. While increasing $p_{N2}/p_T$ from 0 to 23% results in an increase of Al/Ti from 1.33 to 2.01, a further increase in $p_{N2}/p_T$ from 23 to 100% promotes a reduction in Al/Ti from 2.01 to 1.57, respectively, see Fig. 7a. For $p_{N2}/p_T = 23\%$ at which the Al/Ti ratio yields the peak value of 2.01 corresponds to the transition from mixed metallic-nitridic to the poisoned mode, compare Fig. 3a. This suggests that in addition to sputtering losses due to scattering and angular distribution the transition from metallic to nitridic sputtering mode influences the Al/Ti ratio. Hence, the Al/Ti ratio is un-proportionally high for $p_{N2}/p_T$ values between 17 and 27%, where the Ti particles are already mainly poisoning but not the Al particles. Further increasing $p_{N2}/p_T$ results also in nitriding of the Al particles of the target and the Al/Ti ratio decreases again to 1.57 with $p_{N2}/p_T = 100\%$, see Fig. 7a.

Analysis of the XRD results showed that the film obtained with $p_{N2}/p_T = 0\%$ is composed of the tetragonal TiAl phase [51]. Films grown with $p_{N2}/p_T$ of 15 and 17%, corresponding to an Al/Ti ratio of 1.62 and 1.93, respectively, exhibit a single-phased cubic structure, see Fig. 7b. Films grown at $p_{N2}/p_T = 23\%$, and hence containing the maximum Al/Ti ratio of 2.01, exhibit a mixed cubic-hexagonal structure. Further increase in $p_{N2}/p_T$ from 23 to 100% results in increasing intensities of the hexagonal and decreasing intensities of the cubic reflexes, towards an almost single-phase hexagonal structure, although the Al/Ti ratio decreases from 2.01 to 1.57, respectively. This is attributed to the concomitant decrease in deposition rate from 17 to 9 nm/min when increasing $p_{N2}/p_T$ from 23 to 100%. Thereby, the time available for surface-diffusion processes during film growth increases, allowing for phase separation. It is noteworthy, that the calculated deposition rate is increasingly over-estimated with increasing hexagonal phase content due to its lower

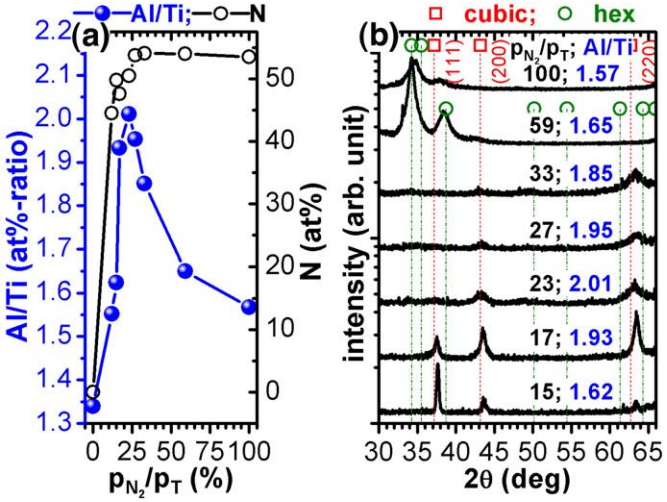


**Fig. 7.** (a) Al/Ti ratio and (b) XRD patterns of the $Ti_{1-x}Al_xN$ thin films as a function of the $N_2$-to-total pressure ratio $p_{N2}/p_T$ (%) with $T_s = 500$ °C, $p_T = 0.4$ Pa, ST = 85 mm, SP = 32 mm, $I_m = 1.5$ A, $B_{ext} = -40$ G, and $E_i = 43$ eV.

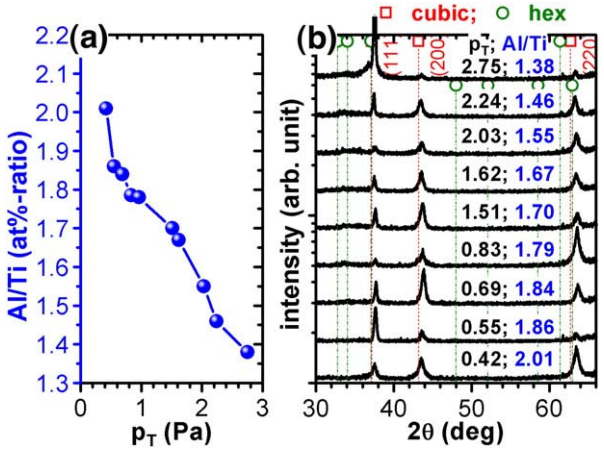


**Fig. 8.** (a) Al/Ti ratio and (b) XRD patterns of the $Ti_{1-x}Al_xN$ thin films as a function of the total pressure $p_T$ (Pa) with $T_s = 500$ °C, $p_{N2}/p_T = 17\%$, ST = 85 mm, SP = 32 mm, $I_m = 1.5$ A, $B_{ext} = -40$ G, and $E_i = 43$ eV.

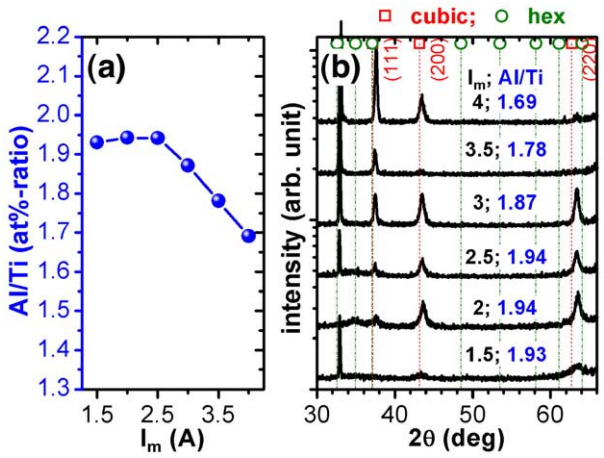


**Fig. 10.** (a) Al/Ti ratio and (b) XRD patterns of the $Ti_{1-x}Al_xN$ thin films as a function of the magnetron power current $I_m$ (A) with $T_s = 500$ °C, $p_{N2}/p_T = 17\%$, $p_T = 0.4$ Pa, ST = 85 mm, SP = 32 mm, $B_{ext} = -40$ G, and $E_i = 43$ eV.

density as compared to the cubic phase used for the estimation of the deposition rate (see the Experimental details section). In addition to the deposition rate, the presence of excess atomic N and/or $N_2^+$ at the film-surfaces during competitive growth can promote hexagonal phase formation at the expense of cubic phases, in agreement to observations of the 001–111-texture development during TiN growth with varying $N_2$-partial pressure [34,52]. The combination of these effects results in the formation of a single-phase hexagonal structure when increasing $p_{N2}/p_T$ to 100%, although the Al/Ti ratio decreases to 1.57 (i.e., $x \sim 0.61$).

A pronounced decrease in Al/Ti ratio by 32.4% from 2.01 to 1.38 of our Ti-Al-N films is obtained when increasing the total pressure from 0.4 to 2.8 Pa, respectively, at a constant $p_{N2}/p_T$ ratio of 17%, see Fig. 8a. This change in Al/Ti ratio of the films towards the target composition by increasing the total pressure suggests increased scattering losses for the lighter Al compared to Ti. Regardless of a decreasing Al/Ti ratio with increasing $p_T$ the structure of the Ti-Al-N films changes from single-phase cubic to binary phased cubic-hexagonal, respectively, see Fig. 8b. This can be attributed to decreased energies of the sputtered Ti and Al particles due to increasing collisions with increasing $p_T$ promoting the deposition rate $R$ to decrease, compare Fig. 2b.

Decreasing the substrate-to-target distance ST from the standard value of 85 mm to 57 mm at a constant low total pressure of 0.4 Pa and $p_{N2}/p_T = 17\%$ results in decreasing Al/Ti ratios from 1.93 to 1.65. A corresponding change in Al/Ti from 2.01 to 1.71 with decreasing ST from 85 to 57 mm is obtained for a higher $p_{N2}/p_T$ of 23%, see Fig. 9a. As the energy of the sputtered species is almost not influenced and the deposition rate even increases, contrary to the previous study with increasing $p_T$, the structure of the films is in agreement to the chemical variation. Hence, the reduction of ST from 85 to 57 mm causes a transformation from the binary cubic-hexagonal phased films towards single-phased cubic films, see Fig. 9b.

Fig. 10a presents the Al/Ti ratio of films deposited at 0.4 Pa with $p_{N2}/p_T = 27\%$ as a function of $I_m$. The composition of the films remains almost stable with increasing $I_m$ from 1.5 to 2.5 A indicating little changes in the target state. Further increase of $I_m$ reduces the poisoning degree of the target as thereby the ratio to $N_2$ increases, compare Fig. 7a. Consequently, in agreement to the study with decreasing $p_{N2}/p_T$ from 27 to 15% the Al/Ti ratio decreases with increasing $I_m$ above 2.5 A as Al particles change from poisoned to metallic mode easier than the Ti particles of our powder-metallurgically prepared $Ti_{0.5}Al_{0.5}$ compound target. As thereby also the deposition rate increases, and hence the time for surface-diffusion processes during film growth and the presence of atomic N or $N_2^+$ on the growing film decreases, the structure of the films changes from binary phased cubic-hexagonal at $I_m = 1.5$ A towards single phased cubic for $I_m = 3$ A, according to the chemical variation, see Fig. 10b.

Fig. 11a shows the compositional response on changing the energy of the ion bombardment. The Al/Ti ratio retains its initial value of 2.04 while increasing the ion energy $E_i$ from 20 to 65 eV. Further increasing

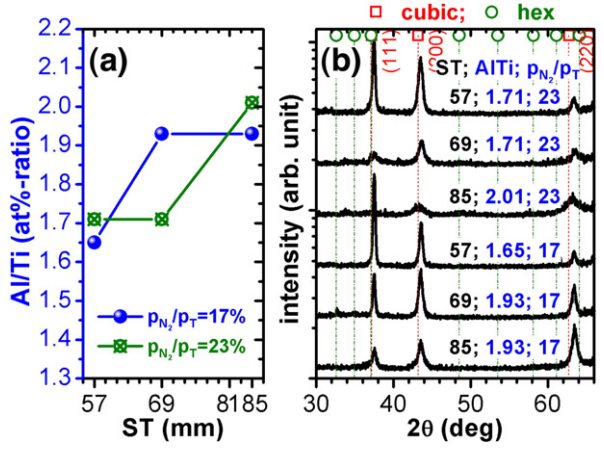


**Fig. 9.** (a) Al/Ti ratio and (b) XRD patterns of the $Ti_{1-x}Al_xN$ thin films as a function of the substrate-to-target distance ST (mm) with $T_s = 500$ °C, $p_{N2}/p_T = 17\%$, $p_T = 0.4$ Pa, SP = 32 mm, $I_m = 1.5$ A, $B_{ext} = -40$ G, and $E_i = 43$ eV.

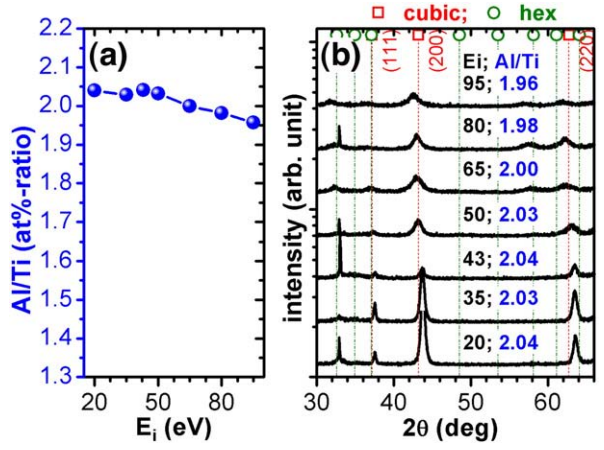


**Fig. 11.** (a) Al/Ti ratio and (b) XRD patterns of the $Ti_{1-x}Al_xN$ thin films as a function of the energy of the bombarding ions $E_i$ (eV) with $T_s = 500$ °C, $p_{N2}/p_T = 17\%$, $p_T = 0.4$ Pa, ST = 85 mm, SP = 32 mm, $I_m = 1.5$ A, and $B_{ext} = -40$ G.

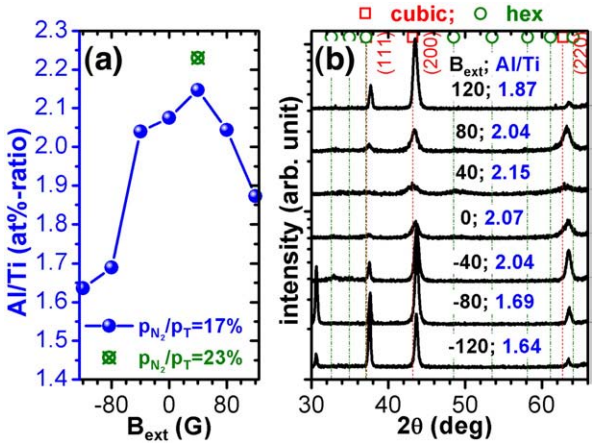


**Fig. 12.** (a) Al/Ti ratio and (b) XRD patterns of the $Ti_{1-x}Al_xN$ thin films as a function of the externally applied magnetic field $B_{ext}$ (G) with $T_s = 500$ °C, $p_{N2}/p_T = 17\%$, $p_T = 0.4$ Pa, ST = 85 mm, SP = 32 mm, $I_m = 1.5$ A, and $E_i = 30$ eV.

$E_i$ to 95 eV causes a slight decrease in Al/Ti to 1.96. This is due to the preferential resputtering of the deposited films, indicated by a decreasing deposition rate from 19 to 18 nm/min, where the higher sputtering yield for Al causes a more pronounced loss in Al. Nevertheless, the structure of the films changes from pronounced cubic (with a small fraction of hexagonal) towards binary cubic-hexagonal, although the Al/Ti ratio decreases with increasing $E_i$. Compared to the cubic, the hexagonal crystals provide easier channeling directions and thus have a higher surviving-probability during energetic ion bombardment with increasing $E_i$. Therefore, increasing $E_i$ results in increased intensities of the hexagonal reflexes and reduced intensities of the cubic reflexes, although the Al/Ti ratio decreases, see Fig. 11a and b.

Applying an external magnetic field $B_{ext}$ strongly influences the ion-to-metal flux ratio $J_{ion}/J_{me}$, the plasma density as well as sputtering area on the target. With an increase in $B_{ext}$ from −120 to +40 G the Al/Ti ratio increases from 1.64 to 2.15. Further increasing $B_{ext}$ from +40 to +120 G results in decreasing Al/Ti ratio from 2.15 to 1.87, respectively. The pronounced increase in $J_{ion}/J_{me}$ from 1.65 to 18.76 (Fig. 4b) with increasing $B_{ext}$ from −40 to +40 G indicates no major correlation to the Al/Ti ratio of the film with a peak value of 2.15 for $B_{ext} = +40$ G. These results further confirm that the different sputter distribution of Al and Ti in addition to the different poisoning state of the $Ti_{0.5}Al_{0.5}$ compound target (Figs. 7 and 10) play a major role in determining the Al/Ti ratio of the film. By increasing $B_{ext}$ from −120 to +120 G the sputtering area of the target decreases and focuses towards the target center. Hence, the sputtering power density increases and for the used substrate position SP = 0 above the target center a pronounced variation in Al/Ti with $B_{ext}$ is obtained. The structure of the films is in good agreement to the Al/Ti variation induced by $B_{ext}$. Films deposited with $B_{ext}$ ranging from −40 to +80 G, having a high Al/Ti ratio between 1.99 and 2.15, exhibit a binary phased cubic-hexagonal structure whereas films with Al/Ti ratios between 1.64 and 1.87 grow single-phase cubic, see Fig. 12b. The peak value in Al/Ti of 2.15 for $B_{ext} = +40$ G can further be increased to 2.23 by increasing $p_{N2}/p_T$ from 17 to 23%, in agreement to an increase in sputtering power density when increasing $B_{ext}$ as thereby the sputtering area of the target decreases.

## 4. Conclusions

Here, we present a detailed study on the effect of varying deposition parameters (i.e., the total working gas pressure $p_T$ from 0.4 to 2.8 Pa, $N_2$-to-total pressure ratio $p_{N2}/p_T$ from 0 to 100%, substrate-to-target distance ST from 57 to 85 mm, substrate position with respect to the center of substrate holder SP from 0 to 80 mm, target current $I_m$ from 1.5 to 4 A, externally applied magnetic field $B_{ext}$ from −120 to +120 G, and ion energy $E_i$ from 20 to 95 eV) on the deposition rate, composition and structure evolution of Ti-Al-N films sputtered from a $Ti_{0.5}Al_{0.5}$ composite target, using a substrate temperature of 500 °C. Due to this variation in deposition conditions the Al/Ti ratio in our films changed between ~1.05 (for $p_T = 4$ Pa, $p_{N2}/p_T = 0$, ST = 85 mm, SP = 32 mm, $I_m = 1.5$ A, $E_i = 43$ V, and $B_{ext} = -40$ G) and 2.15 (for $p_T = 0.4$ Pa, $p_{N2}/p_T = 17\%$, ST = 85 mm, SP = 32 mm, $I_m = 1.5$ A, $E_i = 43$ V, and $B_{ext} = +40$ G). Based on our studies we can conclude that mainly losses due to scattering and angular distribution of the sputter flux together with the different poisoning state of the Ti and Al particles of the powder-metallurgically prepared $Ti_{0.5}Al_{0.5}$ target lead to the huge deviation in Al/Ti ratio of the films as compared to the target.

In particular the different poisoning states of the target constituents account for the broad variation in Al/Ti, which first increases from 1.33 to 2.01 when increasing $p_{N2}/p_T$ from 0 to 23% and then decreases again from 2.01 to 1.57 when increasing $p_{N2}/p_T$ further from 23 to 100%. Scattering losses are responsible for the reduction in Al/Ti ratio from 2.03 to 1.38 when increasing $p_T$ from 0.4 to 2.8 Pa, due to increased effects on the lighter Al atoms. Losses due to the angular distribution of the Ti and Al sputter flux where investigated by increasing SP from 0 to 80 mm, resulting in a decrease of Al/Ti from 2.04 to 1.47. Consequently, the sputter flux exhibits a broader angular distribution for Al than for Ti.

Due to the chemical variation of the Al/Ti ratio in the thin films, induced by the deposition conditions, also their structure changes correspondingly between single-phase cubic, mixed cubic-hexagonal, and single-phase hexagonal. However, the maximum Al content for single-phase cubic $Ti_{1-x}Al_xN$ is strongly determined by the deposition parameters and could be obtained with $x = 0.66$ when using at total pressure of 0.4 Pa, a $N_2$-to-total pressure ratio of 17%, a sputtering power current of 1.5 A, an externally applied magnetic field of −40 G, an energy of the bombarding ions of 43 eV, a substrate-to-target distance of 85 mm and a substrate position of 32 mm. In particular the $N_2$-to-total pressure ratio in combination to the sputtering power density was found to strongly influence the maximum Al content in single-phase cubic structured Ti-Al-N thin films when prepared by sputtering from a powder-metallurgically prepared Ti-Al target.

## Acknowledgements

The financial supports from the START Program (Project Y371) of the Austrian Science Fund (FWF) are greatly acknowledged. Li Chen thanks the Ministry of Education of China for over-sea student fellowship (Grant No. [2007]3020). Yong Du acknowledges Key Project of Hunan Provincial Bureau of Science and Technology of China (Grant No. 2008FJ2007). The authors are grateful to Gerhard Hawranek for performing the EDX measurements.

## References

[1] A.A. Voevodin, P. Stevenson, C. Rebholz, J.M. Schneider, A. Matthews, Vacuum, 46 (1995) 723.
[2] B. Window, N. Savvides, J. Vac. Sci. Technol. A 14 (1986) 196.
[3] B. Window, Surf. Coat. Technol. 71 (1995) 93.
[4] P.J. Kelly, R.D. Arnell, Vacuum 56 (2000) 159.
[5] U. Helmersson, M. Lattemann, J. Bohlmark, A.P. Ehiasarian, J.T. Gudmundsson, Thin Solid Films 513 (2006) 1.
[6] I. Safi, Surf. Coat. Technol. 127 (2000) 203.
[7] J. Musil, P. Baroch, J. Vlček, K.H. Nam, J.G. Han, Thin Solid Films 475 (2005) 208.
[8] S. Berg, T. Nyberg, Thin Solid Films 476 (2005) 215.
[9] W.D. Sproul, D.J. Christie, D.C. Carter, Thin Solid Films 491 (2005) 1.
[10] K. Kutschej, P.H. Mayrhofer, M. Kathrein, P. Polcik, R. Tessadri, C. Mitterer, Surf. Coat. Technol. 200 (2005) 2358.
[11] P.H. Mayrhofer, C. Mitterer, H. Clemens, L. Hultman, Prog. Mater. Sci. 51 (2006) 1032.
[12] M. Pfeiler, K. Kutschej, M. Penoy, C. Michotte, C. Mitterer, M. Kathrein, Int. J. Refract. Met. Hard. Mater. 27 (2009) 502.
[13] M. Moser, P.H. Mayrhofer, Scr. Mater. 57 (2007) 357.
[14] F. Rovere, P.H. Mayrhofer, J. Vac. Sci. Technol. A 25 (2007) 1336.
[15] O. Knotek, M. Böhmer, T. Leyendecker, J. Vac. Sci. Technol. A 4 (1986) 2695.
[16] A. Kimura, H. Hasegawa, K. Yamada, T. Suzuki, Surf. Coat. Technol. 120 (1999) 438.

[17] A. Hörling, L. Hultman, M. Oden, J. Sjolen, L. Karlsson, Surf. Coat. Technol. 191 (2005) 384.
[18] R. Wuhre, S. Kim, W.Y. Yeung, Scr. Mater. 37 (1997) 1163.
[19] J. Willer, S. Pompl, D. Ristow, Thin Solid Films 188 (1990) 157.
[20] C. Mitterer, J. Solid State Chem. 133 (1997) 133.
[21] J.Y. Rauch, C. Rousselot, N. Martin, Surf. Coat. Technol. 157 (2002) 138.
[22] J. Neidhardt, S. Mráz, J.M. Schneider, E. Strub, W. Bohne, B. Liedke, W. Möller, C. Mitterer, J. App. Phys. 104 (2008) 063304.
[23] P.H. Mayrhofer, A. Horling, L. Karlsson, J. Sjolen, T. Larsson, C. Mitterer, L. Hultman, Appl. Phys. Lett. 83 (2003) 2049.
[24] S. PalDey, S.C. Deevi, Mater. Sci. Eng. A 342 (2003) 58.
[25] A. Hörling, L. Hultman, M. Oden, J. Sjölen, L. Karlsson, Surf. Coat. Technol. 191 (2005) 384.
[26] P.H. Mayrhofer, D. Music, J.M. Schneider, J. Appl. Phys. 100 (2006) 094906.
[27] P.H. Mayrhofer, D. Music, J.M. Schneider, Appl. Phys. Lett. 88 (2006) 071922.
[28] P.H. Mayrhofer, F.D. Fischer, H.J. Böhm, C. Mitterer, J.M. Schneider, Acta. Mater. 55 (2007) 1441.
[29] L. Chen, Y. Du, P.H. Mayrhofer, S.Q. Wang, J. Li, Surf. Coat. Technol. 202 (2008) 5158.
[30] K. Kutschej, P.H. Mayrhofer, M. Kathrein, P. Polcik, C. Mitterer, Surf. Coat. Technol. 188–189 (2004) 358.
[31] L. Chen, Y. Du, S.Q. Wang, J. Li, Int. J. Refract. Met. Hard. Mater. 25 (2007) 400.
[32] J.Y. Rauch, C. Rousselot, N. Martin, C. Jacquot, J. Takadoum, J. Eur. Ceram. Soc. 20 (2000) 795.
[33] H. Hasegawa, Y. Kimura, T. Suzuki, Surf. Coat. Technol. 132 (2000) 76.
[34] P.H. Mayrhofer, M. Geier, C. L ö cker, Li Chen, Int. J. Mater. Res. (2009).
[35] J.A. Thornton, J. Vac. Sci. Technol. 15 (1978) 188.
[36] I. Petrov, V. Orlinov, I. Ivanov, J. Kourtev, Contrib. Plasma Phys. 28 (1988) 157.
[37] F. Adibi, I. Petrov, J.E. Greene, L. Hultman, J.E. Sundgren, J. Appl. Phys. 73 (1993) 8520.
[38] C. Mitterer, P.H. Mayrhofer, E. Kelesoglu, R. Wiedemann, H. Oettel, Z. Met.kd. 90 (1999) 602.
[39] I. Petrov, P.B. Barna, L. Hultman, J.E. Greene, J. Vac. Sci. Technol. A 21 (2003) 117.
[40] F. Adibi, I. Petrov, J.E. Reene, U. Wahlsträm, J.-E. Sundgren, J. Vac. Sci. Technol. A 11 (1993) 3283.
[41] S.G. Zotova, R. Kaltofen, T. Sebald, Surf. Coat. Technol. 127 (2000) 144.
[42] L.J. Meng, M.P. Santos, Surf. Coat. Technol. 90 (1997) 64.
[43] S.D. Ekpe, L.W. Bezuidenhout, S.K. Dew, Thin Solid Films 474 (2005) 330.
[44] J.C. Oliveira, A. Manaia, J.P. Dias, A. Cavaleiro, D. Teer, S. Taylor, Surf. Coat. Technol. 200 (2006) 6583.
[45] J. Alami, K. Sarakinos, G. Mark, M. Wuttig, Appl. Phys. Lett. 89 (2006) 154104.
[46] R.K. Waits, J. Vac. Sci. Technol. 15 (1978) 179.
[47] P. Sigmund, Appl. Phys. Lett. 14 (1969) 114.
[48] T. Nyberg, C. Nender, H. Högberg, S. Berg, Surf. Coat. Technol. 94–95 (1997) 242.
[49] W.D. Westwood, Sputter deposition, AVS, New York, 2003.
[50] B.Y. Shew, J.L. Huang, Surf. Coat. Technol. 71 (1995) 30.
[51] Powder Diffraction File, International Center for Diffraction Data, JCPDF-ICDD, 2005.
[52] D. Gall, S. Kodambaka, M.A. Wall, I. Petrov, J.E. Greene, J. Appl. Phys. 93 (2003) 9086.